# Circuit Models for Three-Dimensional Geometrices Including Dielectrics

Albert E. Ruehli, *Fellow, IEEE,* and Hansruedi Heeb, *Member, IEEE*

*Abstract*—**The Partial Element Equivalent Circuit (PEEC) approach has proven to be useful for the modeling of many different electromagnetic problems. The technique can be viewed as an approach for the electrical circuit modeling for arbitrary three dimensional geometries. For example, the "3D transmission line" properties of VLSI interconnects and packages can be modeled. Recently, we extended the method to include retardation with the rPEEC models. So far the dielectrics have been taken into account only in an approximate way. In this paper, we generalize the technique to include arbitrary homogeneous dielectric regions. The new circuit models are applied in the frequency as well as the time domain. The time solution allows the modeling of VLSI systems which involve interconnects as well as nonlinear transistor circuits.**

## I. Introduction

THE SPEED of VLSI systems has increased considerably in the last few years. For high performance systems, the rise time of the signals are well below one nanosecond and the cycle time is rapidly decreasing to take advantage of the increased performance of new technologies. One of the consequences of this is that the accurate electrical modeling of the passive parasitic elements has become more important since the interconnects contribute a large portion to the signal delays. For VLSI systems, other aspects like signal distortion and unwanted signal coupling among the different wires must be accurately predicted since these factors limit the ultimate performance of systems. Recently, other factors like electromagnetic interference (EMI) [1] have become important for VLSI designs. They too require extensive modeling of both circuits and interconnects. The main challenge in all these problems is the complexity of the geometries which must be modeled in order to provide realistic answers.

The topic of VLSI interconnect modeling is relatively recent in comparison to the general area of transmission line modeling. The first work on interconnections focused mostly on two dimensional transmission line models e.g., [2] since the larger structures were described with sufficient accuracy by this type of model for the frequencies of interest. The two dimensional transmission line theory requires that the cross-sections of the conductors remains constant for a distance which is long compared to the cross-sectional dimensions. Today, this approach is still valid for some aspects of VLSI systems like the wires on some printed circuit boards. As the structures have become more miniaturized, the three dimensional aspects have become more important. Progress has been made since then in both the two and three dimensional modeling areas. A large number of references are given in [3] for both two and three dimensional interconnect models. Also, more recently, a relatively large body of work is being performed in the three dimensional modeling in the frequency domain using both finite difference e.g., [4], [5] and integral equation formulations e.g., [6]–[9]. Also, a number of commercially available tools have been created recently aimed at the solution of such problems [10]. The majority of the tools and techniques are for the frequency domain only.

Complexity is one of the main challenges which must be overcome in the solution of these problems. Because the number of transistors and interconnects in VLSI systems is continuously increasing, approximations must be used whenever possible to manage the complexity. Circuit theory is probably the area where complexity has been managed the best by the application of many different model simplification techniques. This motivated us to translate the electromagnetic interconnect problem to the circuit domain. Circuit model simplifications can be divided into two different cases. In the first case, we can set up a simplified model to begin with. For example the small dimensions and the limited distance of the on chip coupling may make the use of retardation unnecessary and the far couplings may be ignored. Also, most of the coupling occurs within a wavelength of the highest frequency. In the second class of approximations, we can replace a complex model by a far simpler one which is sometimes called a macromodel. The AWE technique [11] is one of the approaches where essentially a lower frequency approximation is used to produce a much simpler model which is adequate for the frequencies of interest for the application at hand. In fact, the AWE technique has been applied very recently to some of these geometries [12].

Circuit oriented modeling of electromagnetics problems has a long history [13]. More recent work in this area is based on both differential equations [14] as well as the integral equation formulations [15]. It is interesting to note that most texts e.g. [16] do attempt to give some circuit interpretation of Maxwell's equations. However they only give a rather elementary treatment of the sub-

Manuscript received October 3, 1991; revised March 11, 1992.

The authors are with the T. J. Watson Research Center, 32-106, P.O. Box 218, Yorktown Heights, NY 10598.

IEEE Log Number 9200933.

ject. A comprehensive approach for the circuit modeling of three dimensional geometries is the partial element equivalent approach (PEEC) [15]. One of the useful aspects of PEEC oriented modeling approach is its generality. The models are applicable both in the time and frequency domain. Further, calculations for the partial capacitances (Fig. 1) or coefficients of potential and partial inductances for the model can be performed independently of the actual circuit domain computations [17]–[19] like the transient analysis or the frequency analysis. The approximate implementation of these models is not unique and different representations may be used depending on the problem solved.

The accuracy of the PEEC circuit modeling approach is the same as that of the full-wave solution. In fact, it is very similar to the moment method (MoM) solution [7], with the exception of the local approximation of the currents and the charges. Further, it is well known that the TEM models for two dimensional geometries correspond to an exact solutions for the wave propagation based on static capacitance and inductance computations. Hence, as an approximation, it is possible to employ quasi-static capacitances for the PEEC models for geometries with finite dielectrics [3]. It is obvious that this approximation will lead to errors for sufficiently high frequencies. In fact, the circuit modeling using capacitances is invalid as soon as the retardations become significant. PEEC models which include retarded effects, called rPEEC, have recently been shown to be useful for the circuit modeling of radiation type problems [20]. Our basic approach is to include the retardation by delay sources in both the time and the frequency domain.

In this paper, we give an extension of the PEEC and rPEEC approach. The key new work is that finite dielectric region are included in the formulation without approximations. This makes the models analogous to a *full-wave* solution. The main differences between our models and a full-wave model are that we formulate the problem in the circuit domain and that charges as well as currents are used as unknowns for both the time and frequency domain solutions. This extension of the rPEEC modeling approach is valuable for the solution of many practical problems. Also, from a theoretical point of view, it is an important tool for the study of the couplings between the electric and magnetic field at dielectric interfaces. For example, the sources of coupling can be identified and the magnitude and the nature of this coupling can be studied. Other issues of interest are the modeling of dielectric interfaces with as few additional unknowns as possible to keep the model complexity small. If the dielectrics can be represented with few additional internal nodes, as is the case for thin layers, then the solution is very efficient in term of unknowns.

In Section II we derive the general integral equation formulation with the extension to multiterminal elements and dielectric regions. Sections III and IV is devoted to the derivation of the new rPEEC model and Section V gives results of the application of the method.

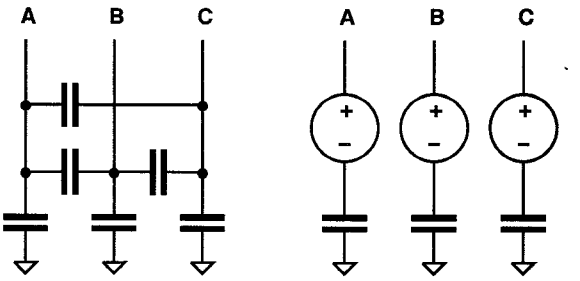


Fig. 1. Representation of the capacitive terms of a circuit with three nodes A, B and C and new equivalent circuit.

## II. Formulation Including Finite Dielectric Regions

### A. Basic Formulation

The interconnection problem we consider here has arbitrary finite size dielectric regions besides the conductors or wires. A simple conductor—dielectric structure is displayed in Fig. 2. We only need to include 4 bodies in our examples since this is sufficient to show all the necessary couplings. Also, we avoid all the rather obvious sums over all the conductors with the benefit of keeping all the equations simple. We start from the work in [15] and use the additional insight on how to include dielectric layers in the moment method solution e.g. [6], [8]. Here, we specifically use approximations of the currents, charges and potentials (voltages) which are appropriate for an equivalent circuit representation. The key idea of the formulation is to model the displacement current due to the bound charges for dielectrics with $\epsilon_r > 1$ separately from the conducting currents due to the free charges [21]. Hence, the Maxwell equation for the dispacement is taken into account as

$$\nabla \cdot \bar{E} = \frac{q^F + q^B}{\epsilon_0} \tag{1}$$

where $q^F$ is the free charge and $q^B$ is the bound charge due to the dielectric regions. The description for the dielectric region is separated in the solution method. To arrive at a consistent equivalent circuit for the static as well as the dynamic case, the dielectric is represented with a three-dimensional mesh of excess capacitances of a value defined in (18). As will be evident below, this leads to a very efficient solution approach.

We write the sum of all the sources of electric field [16] at any point in a conductor

$$\bar{E}_0(\bar{r}, t) = \frac{\bar{J}^C(\bar{r}, t)}{\sigma} + \frac{\partial \bar{A}(\bar{r}, t)}{\partial t} + \nabla \Phi(\bar{r}, t) \tag{2}$$

where $\bar{E}_0$ is an applied electric field (if any), $\bar{J}^C$ is the current density in a conductor, $\bar{A}$ and $\Phi$ are vector and scalar potentials, respectively. The dielectrics are taken into account separately as an equivalent current in a free space environment. This is accomplished through adding and subtracting $\epsilon_0(\partial \bar{E}/\partial t)$ in the Maxwell equation for $\bar{H}$,

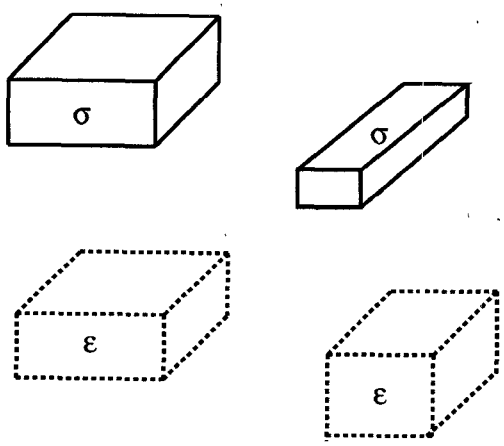


Fig. 2. Illustration of the finite conductor and dielectric problem.

or

$$\nabla \times \bar{H} = \bar{J}^C + \epsilon_0(\epsilon_r - 1)\frac{\partial \bar{E}}{\partial t} + \epsilon_0 \frac{\partial \bar{E}}{\partial t}. \tag{3}$$

Here, the equivalent current in (3) is written as a total current

$$\bar{J}(\bar{r}, t) = \bar{J}^C(\bar{r}, t) + \epsilon_0(\epsilon_r - 1)\frac{\partial \bar{E}}{\partial t} \tag{4}$$

where $\bar{J}^C(\bar{r}, t)$ is the conductor current and the remainder of the equations is the equivalent polarization current due the the dielectrics. We can easily check that (3) and (4) reduce to the standard case for $\epsilon_r = 1$. The vector potential $\bar{A}$ is for a single conductor at a field point $\bar{r}$ given by

$$\bar{A}(\bar{r}, t) = \frac{\mu}{4\pi}\int_{v'} K(\bar{r}, \bar{r}')\bar{J}(\bar{r}', t_d)\, dv' \tag{5}$$

where $v'$ is the volume of the material over which the current density is flowing and the retardation time is given by

$$t_d = t - \frac{|\bar{r} - \bar{r}'|}{c} \tag{6}$$

which simply is the time retarded by the free space travel time between the points $\bar{r}$ and $\bar{r}'$. In the formulation used here, both the retardation and the Greens functions are free space quatities. For convenience and notational clarity we define the Kernel

$$K(\bar{r}, \bar{r}') := \frac{1}{|\bar{r} - \bar{r}'|} \tag{7}$$

Similarly, the scalar potential is

$$\Phi(\bar{r}, t) = \frac{1}{4\pi\epsilon_0}\int_{v'} K(\bar{r}, \bar{r}')q^T(r', t)\, dv' \tag{8}$$

where $q^T = q^F + q^B$. Finally, using the above equations, we can formulate an integral equation for the electric field at a point $\bar{r}$ which is to be located either on a conductor or inside a dielectric region. Starting from (2) with the externally applied electric field set to zero, and substituting for $\bar{A}$ and $\Phi$ from (5) and (8) respectively we get for the field point on a conductor

$$\frac{\bar{J}(\bar{r}, t)}{\sigma} + \frac{\mu}{4\pi}\int_{v'} K(\bar{r}, \bar{r}')\frac{\partial \bar{J}^C(\bar{r}', t_d)}{\partial t}\, dv' + \epsilon_0(\epsilon_r - 1)\frac{\mu}{4\pi}\int_{v'} K(\bar{r}, \bar{r}')\frac{\partial^2 \bar{E}(\bar{r}', t_d)}{\partial t^2}\, dv' + \frac{\nabla}{4\pi\epsilon_0}\int_{v'} K(\bar{r}, \bar{r}')q^T(r', t)\, dv' = 0. \tag{9}$$

The other case we need to consider is the situation when the field point is in a dielectric region with $\epsilon_r > 1$

$$\bar{E}(\bar{r}, t) + \frac{\mu}{4\pi}\int_{v'} K(\bar{r}, \bar{r}')\frac{\partial \bar{J}^C(\bar{r}', t_d)}{\partial t}\, dv' + \epsilon_0(\epsilon_r - 1)\frac{\mu}{4\pi}\int_{v'} K(\bar{r}, \bar{r}')\frac{\partial^2 \bar{E}(\bar{r}', t_d)}{\partial t^2}\, dv' + \frac{\nabla}{4\pi\epsilon_0}\int_{v'} K(\bar{r}, \bar{r}')q^T(r', t)\, dv' = 0. \tag{10}$$

We observe that the form of both equations is the same, with the exception of the local electric field, which is given by the material in which the field point resides. This simplifies the discretization and equivalent circuit interpretations for (9) and (10) which are performed in the next section.

### B. Discretization of Unknowns

The conductor arrangement in Fig. 2 includes the types of conductors and dielectric regions which must be considered for a general formulation of the mixed conductors and dielectrics problem. For clarity we assume that the dielectrics are lossless. To solve the integral equation (9) numerically we choose appropriate approximation for the current, potential and charge variables. We will not use the standard surface approximations which are usually employed for the infinite frequency solution. Conventionally, the current is assumed to flow in a thin surface layer only due to the skin effect approximation which is more suitable for microwave applications. Here, we assume the current flow to be uniform inside a cell of conductor, which leads to a solution which is consistent with the low frequency solution also. Hence, electrically thick conductors must still be further divided if the skin effect is to be modeled accurately. In many practical cases this can be avoided since the conductor thicknesses are often comparable to the skin depth. The charges are on the surfaces of the conductors. The different approximations used for the currents and charges require that we cannot utilize the continuity equation directly to replace the charges by current variables as is done in the conventional moment type solutions [7] in the form

$$\nabla \cdot \bar{J} + \frac{\partial q}{\partial t} = 0. \tag{11}$$

The charges are, in all the solution approaches, assumed

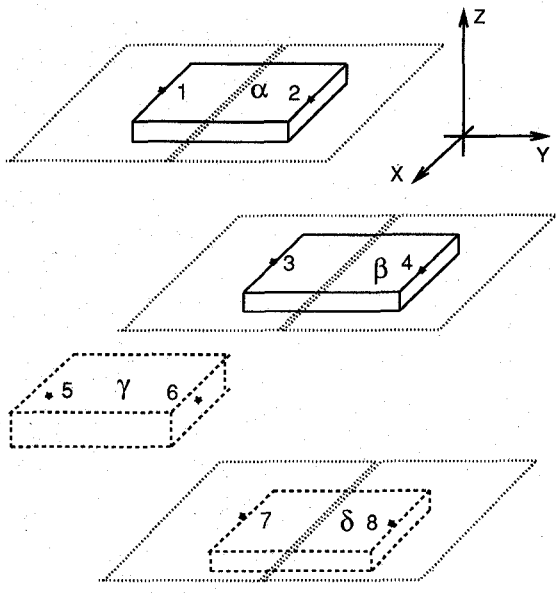


Fig. 3. Cell Structure for finite conductors.

to be located on the conductor surfaces since the relaxation times move the charges "instantaneously" to the conductor surfaces for the high conductivities of the conductors involved. In our approach, we will implement the continuity equation in the form of Kirchoff's current law. This task can be left to the circuit solver which can be a general purpose program like SPICE [22] or ASTAP [23].

The above considerations are used in the actual discretization of the currents and charges as well as the potentials. We divide the conductors up into rectangular cells with a uniform current flow, similar to the conventional approximation for a resistance and partial inductance problems [15], [19]. Hence, the insides of the conductor and the dielectric regions are divided up into "blocks" or "cells" for which we assume that the conduction or displacement currents respectively are uniform. Further, the surfaces of the conductors are completely laid out with capacitive cells to represent the displacement currents. Fig. 3 gives example cells for both conductor and dielectric surfaces which may belong to various surfaces in the geometry shown in Fig. 2. The dotted area cells in Fig. 3 are surface patches for the free or total charge densities, $q^F$ or $q^T$ respectively on the conductors, depending on whether the surfaces touch dielectric regions. All dielectrics needs to be covered with surface cells for bound charge $q^B$. The volume cells in the dielectric regions are the appropriate representation for the polarization currents inside the dielectrics, as will become evident below. The volume parts of the $\alpha$, $\beta$ and $\delta$ cells are located directly under the surface while $\gamma$ is an interior cell.

### C. Discretization of the Integral Equation

In this subsection we will apply the discretizations of the last subsection to the integral equation (9) for the cell structure shown in Fig. 3. The two conductor and dielectric cells shown may be located either on the same or on different bodies. Dielectric cell $\gamma$ is an internal cell and has no outside surface while dielectric cell $\delta$ is on the surface of the dielectric body. Hence, the derivation includes all possible cases. We start by recognizing that three coupled integral equation (I.E.) result if we represent the vector quantities in terms of the Cartesian coordinates. For this case the vector quantities are $\bar{J} = J_x\hat{x} + J_y\hat{y} + J_z\hat{z}$ and $\bar{E} = E_x\hat{x} + E_y\hat{y} + E_z\hat{z}$. Using this, the three I.E. are identical in form with the exception of the space directions $x$, $y$, $z$. Hence, we will consider cells in the $y$-direction only, without loss of generality. This orientation corresponds to the cells shown in Fig. 3. Two different cases must be considered for the general case. In one situation, we locate the field point $\bar{r}$ on a conductor cell e.g. $\alpha$. For the second case the field point $\bar{r}$ must be located on a dielectric cell e.g., $\gamma$. Equation (9) applied to the conductor cell $\alpha$ is

$$\begin{aligned}
&\frac{J_y^C(\bar{r}, t)}{\sigma_\alpha} + \frac{\mu}{4\pi}\int_{v_{\alpha'}} K(\bar{r}, \bar{r}')\frac{\partial J_y^C(\bar{r}', t_d)}{\partial t}\,dv' \\
&\quad + \frac{\mu}{4\pi}\int_{v_{\beta'}} K(\bar{r}, \bar{r}')\frac{\partial J_y^C(\bar{r}', t_d)}{\partial t}\,dv' \\
&\quad + \epsilon_0(\epsilon_\gamma - 1)\frac{\mu}{4\pi}\int_{v_{\gamma'}} K(\bar{r}, \bar{r}')\frac{\partial^2 E_y(\bar{r}', t_d)}{\partial t^2}\,dv' \\
&\quad + \epsilon_0(\epsilon_\delta - 1)\frac{\mu}{4\pi}\int_{v_{\delta'}} K(\bar{r}, \bar{r}')\frac{\partial^2 E_y(\bar{r}', t_d)}{\partial t^2}\,dv' \\
&\quad + \frac{1}{4\pi\epsilon_0}\int_{S_{\alpha'}} \frac{\partial}{\partial y} K(\bar{r}, \bar{r}')q^T(r', t_d)\,ds' \\
&\quad + \frac{1}{4\pi\epsilon_0}\int_{S_{\beta'}} \frac{\partial}{\partial y} K(\bar{r}, \bar{r}')q^T(r', t_d)\,ds' \\
&\quad + \frac{1}{4\pi\epsilon_0}\int_{S_{\delta'}} \frac{\partial}{\partial y} K(\bar{r}, \bar{r}')q^T(r', t_d)\,ds' = 0. \qquad (12)
\end{aligned}$$

Again, we choose $\gamma$ to represent a dielectric cell interior to the dielectric while $\delta$ is a half cell [15] directly under the surface in the dielectric block. The surface cell represents the surface bound charge on the dielectric. In accordance with (10) the case where the field point is located in the dielectric has the term $J/\sigma$ replaced by $E(\bar{r}, t)$. This is under the assumption that the dielectric is lossless. The lossy dielectric case is given by the combination of both terms.

## III. Partial Element Equivalent Circuit Models

In this section, we will extend the PEEC and rPEEC modeling approaches for dielectric regions *without* approximations with the exception of the discretizations. The aim is to set up a set of circuit equations or equivalent circuits where the unknowns are potentials as well as currents. Potentials correspond to voltages with the reference node corresponding to the "node" at infinity. We use the geometry in Fig. 2 to develop the circuit representation

of the conductors and the dielectrics. In fact, we show that the *same* conventional frequency independent circuit elements can be used in the new model which are employed in the original PEEC and rPEEC models.

The coupling to a conductor cell by all the cell types is considered first. We start the derivation by integrating each term of the I.E. (12) over the volume $v_\alpha$ of the conductor cell $\alpha$ in Fig. 3

$$\frac{1}{a_\alpha}\int_{v_\alpha} f(\bar{r})\, dv = \frac{1}{a_\alpha}\int_{a_\alpha}\int_{l_\alpha} f(\bar{r})\, da\, dl \tag{13}$$

where $v_\alpha$ is the volume of the conductor cell, $\alpha$, $a_\alpha$ is the cross-section of the cell ($x$-$z$ direction) and $l_\alpha$ is the length ($y$-direction) and $f(\bar{r})$ is the integrand. The surface cells are integrated appropriately. This corresponds to averaging the field point $\bar{r}$ over the cell volume $v_\alpha$. Our method corresponds to a Galerkin solution which is well known to have a positive impact on the solution accuracy. However, additional integrations must be performed in comparison to point or line matching. We found that our solution method is numerically very robust especially since we use predominantly analytic integration for the coefficient computation.

After applying the integration to (12), we can assert what the appropriate equivalent circuit is for each term of the I.E.. The first term of the I.E. can easily be shown to be the resistance of the cell $R_\alpha$ with the dc current $I_y^C = (\phi_1 - \phi_2)/R_\alpha$ since the current through the cell is $I_y = J_y a_\alpha$. The resistance is as usual

$$R_\alpha = \frac{l_\alpha}{\sigma a_\alpha} \tag{14}$$

The second term applies also to the field point cell $\alpha$ and its voltage drop adds to the resistance the cell. For both the second and third terms in (12) we make use of the laminar, uniform current flow through the cell to take

$$\frac{\partial J_y}{\partial t} = \frac{1}{a_y}\,\partial I_y/\partial t \tag{15}$$

outside the integral. With some help from [19], we recognize that the second term represents the partial self inductance of the conductor cell $\alpha$ where the partial inductance between two parallel cells $\alpha$ and $\beta$ with parallel current flow is given by

$$Lp_{\alpha\beta} = \frac{\mu}{4\pi}\frac{1}{a_\alpha a_\beta}\int_{v_\alpha}\int_{v_\beta} K(\bar{r}_\alpha, \bar{r}_\beta)\, dv_\alpha\, dv_\beta. \tag{16}$$

For the rectilinear coordinates considered here, all nonparallel cells are perpendicular for which the partial mutual inductances are zero. Hence, the second and third terms in (12) are simply interpreted as

$$Lp_{\alpha\alpha}\frac{dI_\alpha}{dt} + Lp_{\alpha\beta}\frac{dI_\beta}{dt} \tag{17}$$

where the first term is the partial self inductance of the cell $\alpha$ and the second term represents the inductive coupling to cell $\alpha$ from a current in the cell $\beta$.

We best consider the case where the field point is located inside the dielectric for the circuit interpretation of terms four and five since this leads to the self terms for these cells. We start with (10) and state the result as a theorem for clarity, before giving a proof. First, we need to define the excess capacitance of a dielectric cell. We resort to Fig. 3 for the illustration of the symbols used in the following definition.

*Definition 1:* The excess capacitance $C_\gamma^+$ of a dielectric cell $\gamma$ is defined as

$$C_\gamma^+ := \frac{\epsilon_0(\epsilon_\gamma - 1)a_\gamma}{l_\gamma} \tag{18}$$

where $\epsilon_\gamma$ is the dielectric constant of the cell, $a_\gamma$ is the cross-section and $l_\gamma$ is the length of the cell.

Surprisingly, we need to extend the concept of partial inductances to include the case where one or both "conductors" are dielectric cells rather than a conductor cells! This is necessary for the circuit interpretation of the volume integrals for cells $\gamma$ and $\delta$ in (12). The theorem below states the result for the dielectric cells.

*Theorem 1:* The voltage across a dielectric cell $\gamma$ with the potentials $\Phi_5$ and $\Phi_6$ applied to the nodes at the ends of the cell is given by

$$\begin{aligned}\Phi_5 - \Phi_6 &= v_L + v_C\\ v_L &= Lp_{\gamma\gamma}\frac{\partial}{\partial t}\left[C_\gamma^+\frac{\partial v_C}{\partial t}\right]\\ i_C &= C_\gamma^+\frac{\partial v_C}{\partial t}.\end{aligned} \tag{19}$$

Theorem 1, is proven by starting with the I.E. for the dielectric case, (10), where we take the y-components the same way as in (12) and where the field point is on the $\gamma$ cell. Here, we only give the relevant terms which are different from the $\alpha$ case. The two terms for cell $\gamma$ are

$$E_y + \epsilon_0(\epsilon_\gamma - 1)\frac{\mu}{4\pi}\int_{v_\gamma} K(\bar{r}, \bar{r}')\frac{\partial^2 E_y(\bar{r}', t_d)}{\partial t^2}\, dv'. \tag{20}$$

We integrate this over the cell $\gamma$, or

$$\frac{1}{a_\gamma}\int_{v_\gamma} f(\bar{r})\, dv = \frac{1}{a_\gamma}\int_{a_\gamma}\int_{l_\gamma} f(\bar{r})\, da\, dl. \tag{21}$$

The first term, which is the total field, integrates to $v_C$, where the relation for $v_C$ is given in differential form as $i_C = C_\gamma^+\, dv_C/dt$. However, additionally an inductive voltage drop is induced in $\gamma$ by the partial self-inductance of the cell $Lp_{\gamma\gamma}$ where $v_L = Lp_{\gamma\gamma}\, di_C/dt$. Note that in this case the current is again correctly $i_C$ for the excess capacitance. Finally, the equivalent circuit for the dielectric is established as $C_\gamma^+$ in series with $Lp_{\gamma\gamma}$. The coupling to other cells is through the partial mutual inductances as is evident from the I.E.s.

The surface integrals in (12) over $S'_\alpha$, $S'_\beta$, and $S'_\delta$ are the conventional coefficients of potential and they need

little new explanations. In this formulation, they all correspond to free space coupling terms as in [15]. The next section will present an alternative formulation for the capacitive part of an rPEEC model needed for retardation.

The best way to show a complete new PEEC equivalent circuit is by example. Specifically, the first example below, which is the dielectric cube in Fig. 4, gives the new models presented in this paper.

## IV. Equivalent Circuit Models

As mentioned above, a key issue in the PEEC modeling approach is how the capacitances are included in the equivalent circuit models. In fact, the concept of capacitance matrices is invalid for the case where retardation is significant. For this case, the coefficients of potential need to be modeled. This is accomplished by representing the potential coefficients by controlled sources. Assuming that $K$ capacitive cells are involved in the problem, then the potential $\Phi_i$ on conductor $i$ is given by

$$\Phi_i(t) = \sum_{j=1}^{K} p_{ij} Q_j(t'_{ij}) \tag{22}$$

where $Q_j$ is the charge on conductor $j$ and the time retardation is

$$t'_{ij} = t - \frac{R_{ij}}{c} \tag{23}$$

where $R_{ij}$ is the distance between conductor $i$ and $j$ and $c$ is the speed of light. If $t'_{ij} = t$ (no retardation) the above equation can be inverted into the short circuit capacitance matrix. However, this may not be a good strategy even for this case since the inversion is taking place "automatically" in the circuit solver when the Jacobian matrix is solved.

It is possible to construct a circuit model using only the *coefficients of potential* $p_{ij}$. The model [24] replaces the capacitances with *pseudo-capacitances* to ground $c'_i = 1/p_{ii}$ and with controlled voltage sources for the coupling

$$U_i^{(c)}(t) = \sum_{j \neq i} \frac{p_{ij}}{p_{jj}} \Phi'_j(t'_{ij}) \tag{24}$$

where $\Phi'_j$ is the potential at the pseudo-capacitance $j$, as shown in Fig. 1. The left hand side shows the capacitance for a circuit with three nodes (A, B, and C) and the right side shows the equivalent circuit model in terms of capacitance and equivalent sources.

The partial inductances are handled in a very similar way by a partial self inductance $Lp_{jj}$ in series with a voltage source $U_i^{(L)}(t)$:

$$U_i^{(L)}(t) = \sum_{j \neq i} \frac{Lp_{ij}}{Lp_{jj}} v'_j(t'_{ij}) \tag{25}$$

where $v'_j$ is the voltage at the partial self inductance $Lp_{jj}$. From the above, we can see how to models all parts of an equivalent circuits in terms of self-capacitance and in terms of (potentially retarded) coupling sources.

Once the equivalent circuit models have been formed, the circuit equations can be set up by the standard approaches for the systematic formulation underlying a circuit solver like the modified nodal analysis (MNA) [25] or sparse tableau approach [23]. The difference to conventional circuit analysis is that the retarded equations are delayed differential algebraic system (DDAE) rather than ordinary differential algebraic systems (DDE). In order to represent the DDAE in a circuit simulator like ASTAP we had to implement a history mechanism [20].

## V. Results

The first example is designed to enhance the impact of the dielectric material on the solution, since the finite dielectric model is the main contribution of this paper. In general, we observed very good convergence of the solution with the number of cells since our approach corresponds to a Galerkin solution with the integration over the field point cells. Also, we used analytical integration for the potential coefficients and mostly analytical integration for the partial inductances where the numerical accuracy of the coefficients was achievable similar to [19]. All the far coefficients are approximated by simple point and line sources with careful attention to the solution accuracy.

Fig. 4 shows an example of a dielectric cube of $\epsilon_r = 5$. The size of the cube is $3 \times 3 \times 3$ cm and a U-shaped conductor is wrapped around three sides. To introduce asymmetry, the top is only half covered by metal. The half covered surface is in the positive $z$-direction while the fully covered sides are in the negative $z$-direction (bottom) and in the negative $y$-direction (left). This surface is divided into two parts by an infinitesimal gap as is evident from Fig. 4. The gap is excited in the middle by a unit voltage source. Again, the purpose of this example is to emphasize the impact of the polarization currents in the dielectric on the result.

Fig. 5 shows schematically the new rPEEC model for the dielectric cube example, where the partial inductances are shown as black rectangles only. Also, the coupling terms for the coefficients of potential are not shown for clarity. In Fig. 6 we used a quasi-static capacitance approximation for the dielectric block. Since these capacitances are mapped in with the free space cofficients of potential, they are not shown and only the conductor model is visible.

Further, we did not take the small resistance into account for the wide conductor. As a further simplification, the PEEC models show only one division for the width of the conductors in the cube problem. All the partial mutual inductances in the same direction are coupled.

Fig. 7 shows the electric field $E_\theta$ of the dielectric cube at 200 MHz in a distance of three meters for $\phi = 90$. The upper solid curve shows the results of the rPEEC model using the quasi-static capacitance approximation corresponding to Fig. 6. The solution for the new rPEEC model (lower solid curve) agrees closely with the dashed curve

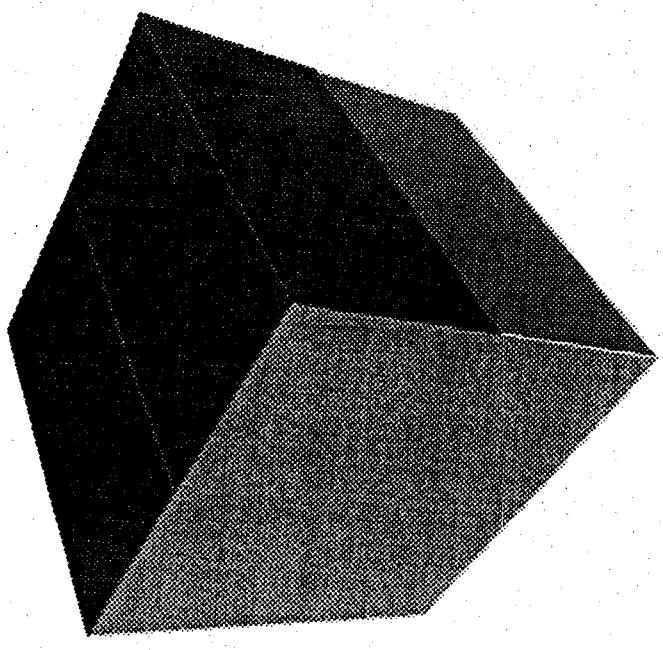

Fig. 4. The dielectric cube example. Metal covers the "bottom," "left" and half of the "top" of the cube. The source is in the infinitesimal gap on the "left" face of the cube.

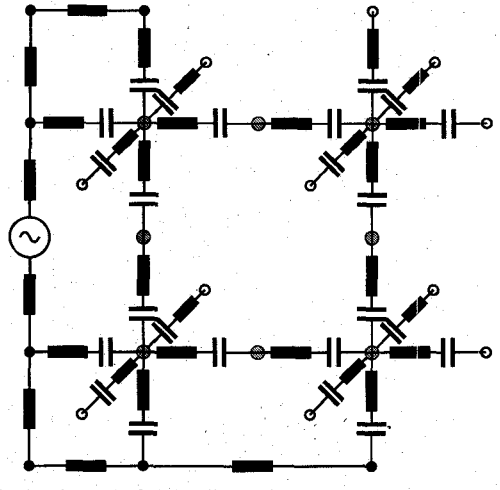

Fig. 5. A circuit mode for the dielectric cube example. The black rectangles represent partial inductances. The black circles are circuit nodes on conductors, the gray circles are internal dielectric nodes and the white circles are dielectric surface nodes. Note shown are the capacitive cross-couplings between the various nodes nor are partial mutual inductances.

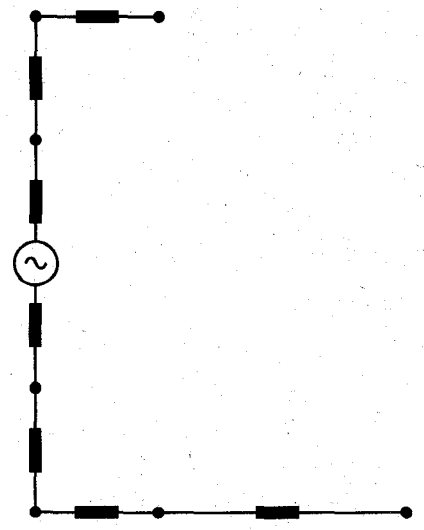

Fig. 6. The quasi-static PEEC model for the dielectric cube. Capacitive cross-coupling are not shown nor are partial mutual inductances.

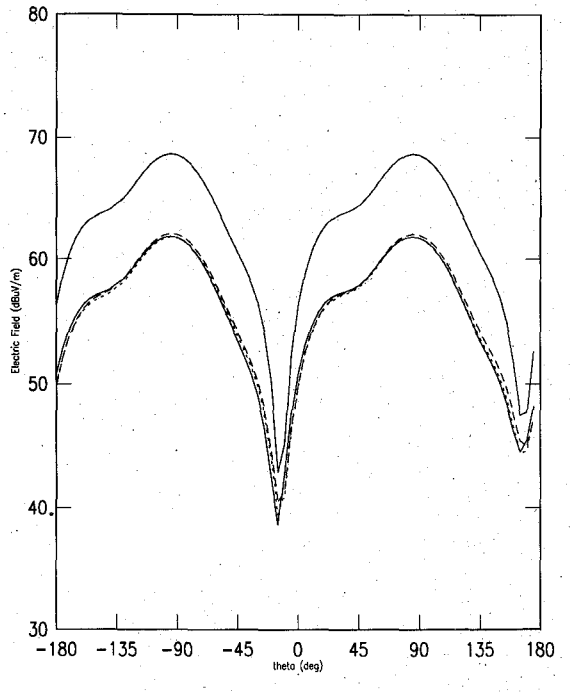


Fig. 7. The electric field $E_\theta$ of the dielectric cube at 200 MHz and $\phi$ 90 degrees. The upper solid curve is the field calculated using a quasi-static dielectric model. The lower three curves show the field calculated with the new circuit model (solid), with a method of moments volume formulation (dashed) and a method of moments surface formulation (dotted).

which is a method of moments (MoM) solution due to [8]. Further, we compared our solution with a MoM surface formulation code [26]. This result is shown in the dotted curve which is in close agreement with our rPEEC result. As a second numerical experiment for the dielectric cube, we compared the impedance of the cube at the source terminals. This is a very sensitive measurement for this example. Fig. 8 shows the source impedance as a function of frequency. Again, the new dielectric model shows excellent agreement with the MoM solver [8], while the quasi-static capacitance model is somewhat in error as expected. Similar results have been observed for other examples.

To illustrate our new time domain computation facility we use the same example cube in Fig. 4. However, the sinusoidal source is replaced by a ramp function with rounded edges with a series resistance of 100 Ω. The rise time of the ramp is 0.1 ns and the response between the outer edges of the conductors (on top and bottom) is shown in Fig. 9. Note that the same rPEEC model was used for both the time as well as the frequency domain. This gives us confidence that the time domain results are correct since we cannot compare them to the other techniques.

As a second time domain example we give the response

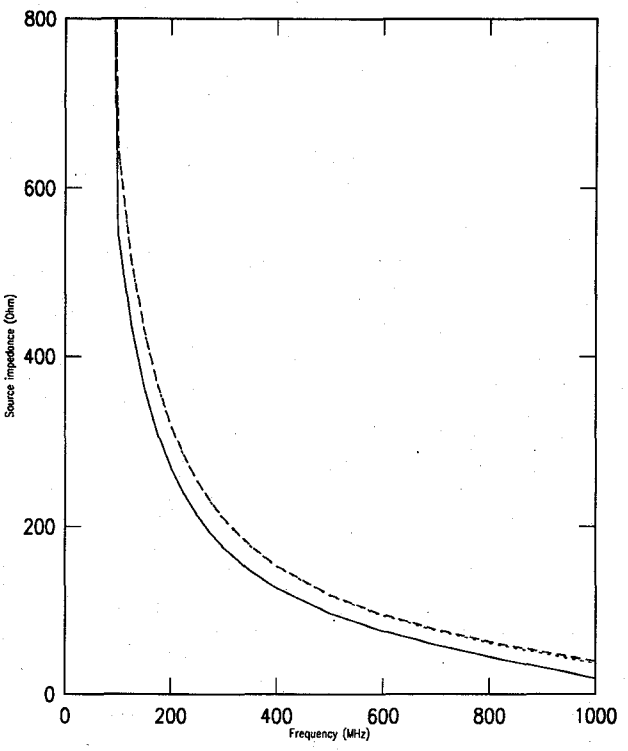


Fig. 8. The source impedance of the dielectric cube. The solid curve shows the quasi-static dielectric model, the dashed and dotted curves, which are mostly on top of each other, show the new dielectric model and a method of moments result.

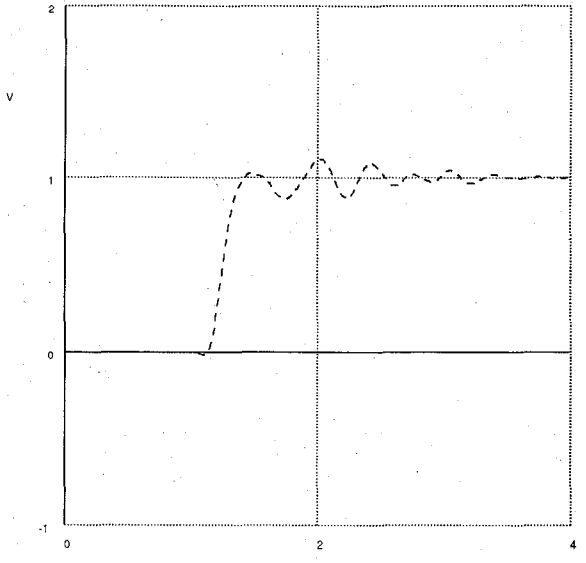


Fig. 9. The time-domain voltage between top and bottom metal (outer edges) of the dielectric cube for a 1 V step excitation with 0.1 ns rise-time.

of a wire or trace on a printed circuit board driven by a standard TTL 74F04 chip driver. The length of the wire is 15 cm the length of the board is 28 cm. Further, the wire is loaded by another TLL 74F04 circuit. Detailed equivalent circuits for both TTL inverters are used. Further, the IC pins and sockets and the vias were modeled with PEEC models in addition to the trace. Fig. 10 shows the driver package model with the pins. Fig. 11 shows a schematic rPEEC equivalent circuit for a part of the socket and package. We excited the integrated circuit driver with a 50 MHz rounded trapezoidal waveform. Fig. 12 shows two waveforms, one at the output of the driver, measured inside the IC package while the other is measured at the end of the trace, inside the receiving IC package. As we demonstrated before [27], the radiation from such a structure can be computed from the time domain results using fast Fourier transform techniques. Fig. 13 finally shows the radiation at three meters from this circuit.

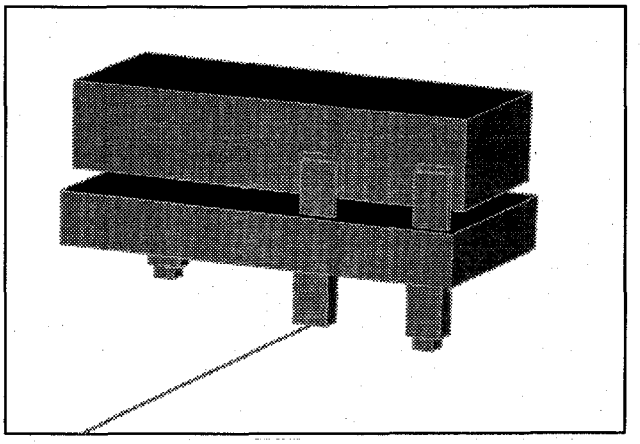

Fig. 10. The driving chip of example two. The power- and ground-planes and the board epoxy have been delected from the picture for better visibility. The figure shows the 74F04 (with pins 1, 12, and 14) and its socket, part of the trace on the PCB and the two vias to the ground- and power planes.

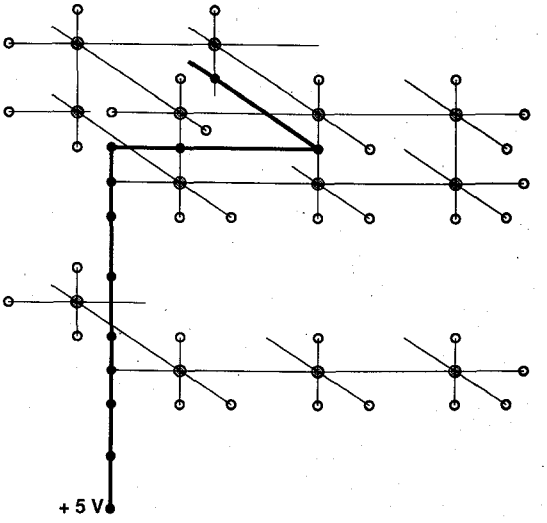


Fig. 11. Part of an rPEEC model of example two. Wide lines are partial inductances (conductors), thin lines partial inductances with a series capacitance (dielectrics). Not shown are the cross-couplings. Solid nodes are metal nodes, grey nodes are internal dielectric nodes and white circles are dielectric surface nodes. The figure shows the power pin and some internal wiring, the corner of the chip case and the corner of the socket.

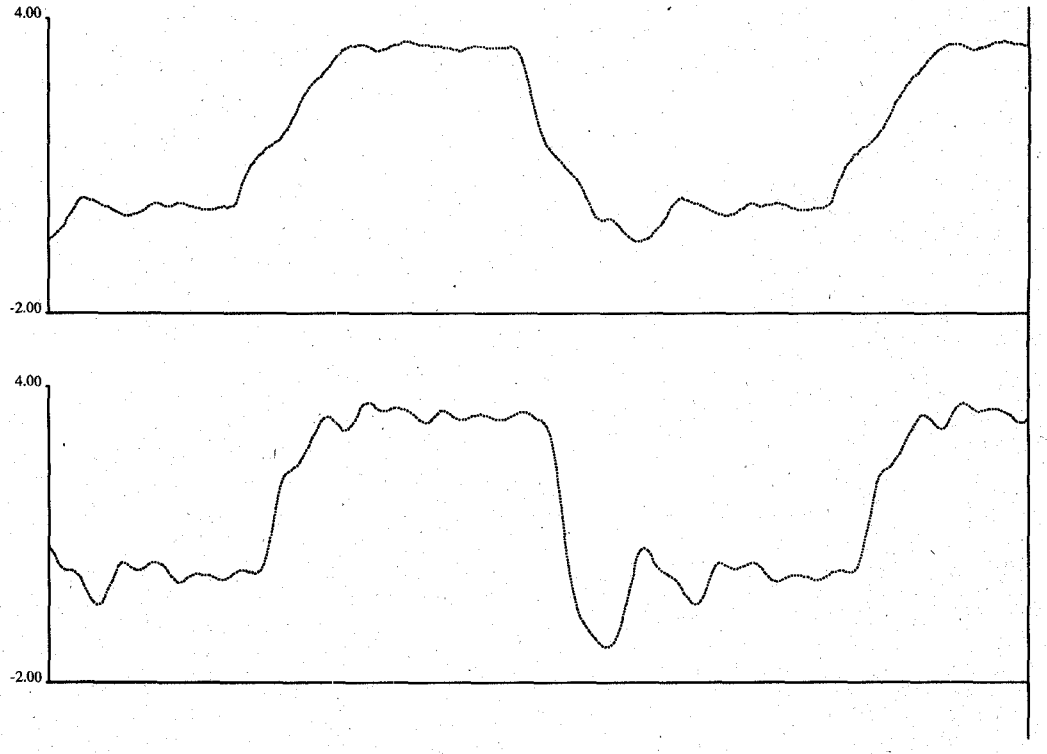


Fig. 12. The waveforms at the source (top) and load end (bottom) of the trace. The horizontal axis runs from about 10 to 42 ns.

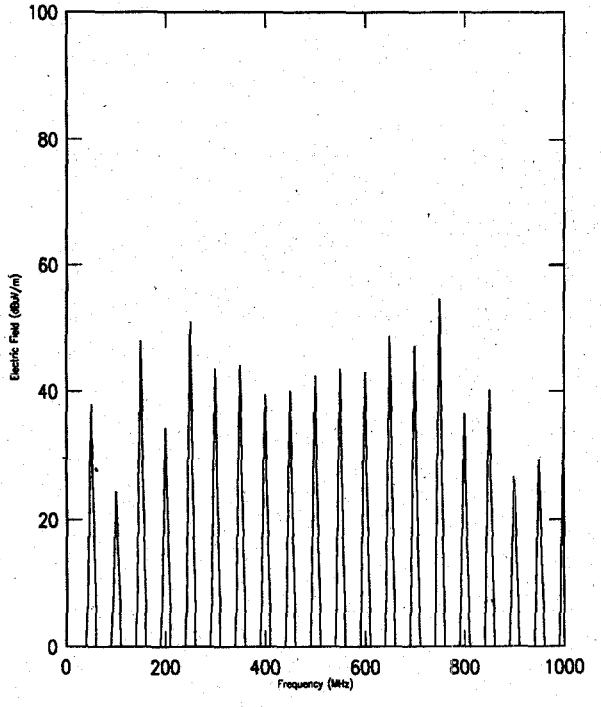


Fig. 13. The simulated radiation of the example in dB/$\mu$V three meters from the PCB.

## VI. Conclusion

The work presented in this paper extends the PEEC and rPEEC circuit modeling technique to an exact full wave solution approach for problems with finite dielectrics. As we demonstrated by the examples, the rPEEC circuit model has many advantages especially if it is used in conjunction with a general purpose, flexible time and frequency domain circuit simulator like ASTAP. Also, circuit approximation can be used to simplify the solution approach such that larger problems can be solved. Further, we gained much insight into many difficult problems by solving them in both the frequency and the time domain.

## Acknowledgment

Insight into the issues at hand has been gained from many discussion meetings with our co-workers S. Daijavad, J. Janak, W. Pence, S. Ponnapalli and B. Rubin.

## References

[1] C. R. Paul, *Introduction to Electromagnetic Compatibility*. New York: Wiley, 1992.
[2] R. Matick, *Transmission Lines for Digital and Communication Networks*. New York: McGraw-Hill, 1969.
[3] A. E. Ruehli, "Survey of computer-aided electrical analysis of integrated circuit interconnections," *IBM J. Res. Devel.*, vol. 23, pp. 626–639, Nov. 1979.
[4] A. Taflove and M. E. Brodwin, "Numerical solution of steady-state electromagnetic scattering problems using the time-dependent Maxwell's equation," *IEEE Transactions Microwave Theory Tech.*, vol. 23, pp. 623–630, Aug. 1975.
[5] R. Mittra and J. F. Lee, "Direct Maxwell's equations solvers in time

and frequency domain—A review," in *Proc. Directions in Electromagnetic Wave Modeling*. New York: Plenum, Oct. 1990.
[6] J. Richmond, "Digital computer solutions of rigorous equations for scattering problems," *Proc. IEEE*, vol. 53, pp. 796–804, Aug. 1965.
[7] R. F. Harrington, *Field Computation by Moment Methods*. New York: Macmillan, 1968.
[8] B. J. Rubin and S. Daijavad, "Radiation and scattering from structures involving finite-size dielectric regions," *IEEE Trans. Antennas Propagat.*, vol. 38, no. 11, pp. 1863–1873, 1990.
[9] J. Nachamkin, S. Ponnapalli, and T. K. Sarkar, "An iterative technique based on the method of least squares applied to scattering problems using the k-space approach," *J. Electromagnetic Waves and Applications*, vol. 5, no. 6, pp. 637–652, 1991.
[10] D. G. Swanson Jr., "Simulating EM fields," *IEEE Spectrum*, vol. 28, pp. 34–37, Nov. 1991.
[11] L. T. Pillage and R. A. Rohrer, "Asymptotic waveform evaluation for timing analysis," *IEEE Trans. Computer-Aided Design*, vol. 9, no. 4, pp. 352–366, 1990.
[12] A. E. Ruehli, H. Heeb, E. Bracken, and R. Rohrer, "Three dimensional circuit oriented electromagnetic modeling for VLSI interconnects," in *Proc. Packaging, Interconnects, Optoelectronics for the Design of Parallel Computers Workshop*, Mar. 1992.
[13] D. Vitkovitch, *Field Analysis*. New York: Van Nostrand, 1966.
[14] P. B. Johns and R. L. Beurle, "Numerical solution of 2-dimensional scattering problems using a transmission-line matrix," *Proc. IEEE*, vol. 59, pp. 1203–1208, Sept. 1971.
[15] A. E. Ruehli, "Equivalent circuit models for three dimensional multiconductor systems," *IEEE Trans. Microwave Theory Tech.*, vol. MTT-22, pp. 216–221, Mar. 1974.
[16] S. Ramo, J. R. Whinnery and T. Van Duzer, *Fields and Waves in Communication Electronics*. New York: Wiley, 1965.
[17] J. F. Janak, D. D. Ling, and H.-M. Huang, "C3DSTAR: A 3D wiring capacitance calculator," in *Proc. IEEE Int. Conf. on Computer Aided Design*, 1989, pp. 530–533.
[18] K. Nabors and J. White, "FastCap: A multipole accelerated 3D capacitance extraction program," *IEEE Trans. Computer-Aided Design*, vol. 10, pp. 1447–1459, Nov. 1991.
[19] A. E. Ruehli, "Inductance calculations in a complex integrated circuit environment," *IBM J. Res. Dev.*, vol. 16, pp. 470–481, Sept. 1972.
[20] H. Heeb, A. Ruehli, "Retarded models for PC board interconnects—or how the speed of light affects your SPICE circuit simulation," in *Proc. IEEE Int. Conf. Computer Aided Design*, Nov. 1991, pp. 70–73.
[21] R. Plonsey and R. Collin, *Principles and Applications of Electromagnetic Fields*. New York: McGraw-Hill, 1961.
[22] L. W. Nagel, "SPICE2: A computer program to simulate semiconductor circuits," Electr. Res. Lab. Report ERL M520, University of California, Berkeley, May 1975.
[23] W. T. Weeks, A. J. Jimenez, G. W. Mahoney, D. Mehta, H. Qua-semzadeh, and T. R. Scott, "Algorithms for ASTAP—a network analysis program," *IEEE Trans. Circuits Theory*, vol. CT-20, pp. 628–634, Nov. 1973.
[24] H. Heeb and A. Ruehli, "Approximate time-domain models of three-dimensional interconnects," in *Proc. IEEE Int. Conf. on Computer Design*, 1990, pp. 201–205.
[25] C.-W. Ho, A. E. Ruehli and P. A. Brennan, "The modified nodal approach to network analysis," *IEEE Trans. Circuits Syst.*, vol. 22, pp. 504–509, June 1975.
[26] S. Ponnapalli and H. Heeb, "EMI prediction using a full-wave analysis method based on a surface formulation," in *Proc. Topical Meeting on Electrical Performance of Electronic Packaging*, Apr. 1992.
[27] H. Heeb, A. Ruehli, J. Janak, and S. Daijavad, "Simulating electromagnetic radiation of printed circuit boards," in *Proc. IEEE Int. Conf. on Computer Aided Design*, 1990, pp. 392–395.

**Albert E. Ruehli** (M'65–SM'74–F'84) was born in Zürich, Switerland. He received his doctorate degree in electrical engineering in 1972 from the University of Vermont.

He has worked at IBM on many different projects, which include mathematical analysis, semiconductor circuits and devices as well as VLSI design. Presently, he is at the IBM T. J. Watson, Research Center, Yorktown Heights NY where he has been manager since 1978 of a computer aided design group.

In 1984 he was technical chairman of the ICCD'84 International Conference on Computer Design: VLSI in Computers, Rye Brook, NY, and he was general chairman of the ICCD'85 conference. In 1975, 1978, and 1982, he received IBM Outstanding Contribution Awards, and in 1982 he received the Guillemin-Cauer prize paper award from the IEEE Circuits and System Society for his work on waveform relaxation. He is the editor of two books entitled Circuit Analysis, Simulation and Design, North Holland 1986, 1987.

**Hansruedi Heeb** (S'87–M'88) received the diploma in physics from the Swiss Federal Institute of Technology (ETH), Zürich, Switzerland in 1982 and the Ph.D. in computer science from the same university in 1988. Since 1989 he is with the IBM T. J. Watson Research Center, Yorktown Heights, NY. His research interests include electromagnetic interference prediction, interconnect modeling and VLSI module generation.